JOURNAL OF COMPUTATIONAL PHYSICS 100, 38–49 (1992)

Explicit Adaptive-Grid Radiation-Magnetohydrodynamics

OSMAN YASAR AND GREGORY A. MOSES

Department of Nuclear Engineering and Engineering Physics, University of Wisconsin-Madison, 1500 Johnson Drive, Madison, Wisconsin 53706

Received July 13, 1990; revised December 13, 1990

An explicit adaptive-grid finite differencing method for one-dimensional radiation-magnetohydrodynamics computations is described. Based on the equidistribution principle, this explicit procedure moves the grid points to regions with high spatial gradients in physical quantities, such as temperature, mass density, pressure, and momentum. The governing magnetic field, radiative transfer, and hydrodynamics equations are transformed to the moving adaptive reference frame. The time and spatially dependent radiation field is determined by solving the radiative transfer equation with the multigroup discrete ordinate S_N method with implicit time differencing. The magnetic field is solved through a diffusion equation resulted from Maxwell's equations and Ohm's law. The field equations are solved using a first-order upwind spatial differencing and explicit time differencing scheme. The coupling between the fluid and radiation field is treated explicitly by first solving for the radiation field and then the fluid equations. A conservative differencing scheme based on the control volume approach is chosen to retain the conservative nature of the governing equations. © 1992 Academic Press, Inc.

1. INTRODUCTION

Radiation processes and radiation transport play an important role in inertial confinement fusion (ICF). The dynamics of target implosions can be strongly affected by radiative transfer. The *indirect drive* approach for target design purposely converts the driver beam energy in the form of laser light or ion beams to X rays and uses these X rays to drive the implosion. A background gas in the ICF target chamber is important for transporting light ion beams from the final driver element to the target. Light ion beams with their high charge to mass ratio and high current densities, cannot propagate over large distances in a vacuum without significant beam divergence. One solution to this, first proposed by Yonas [1], is to fill the standoff region with a gas and strike a discharge along the path from the diode to the target. This gas is preconditioned by passing a current through it to form a long magnetized plasma between the ion diode and the target to confine the ion beams as shown in Fig. 1. Radiative transfer can play an important role during the formation of this z-discharge plasma channel. It certainly plays a role as an ion beam passes through and heats the plasma channel. The gas in the target chamber also interacts with the exploding target as shown in Fig. 2, creating a so-called microfireball. These hot and dense plasmas emit and reabsorb radiation at soft X-ray energies (1–1000 eV). The radiation represents a significant energy transfer mechanism in the plasma, thus the coupling between the plasma and the radiation field must be accurately determined to predict and interpret the outcome of ICF experiments.

Previous studies involved modeling these target chamber problems on a lagrangian grid system with the radiative transfer represented by a diffusion equation [2–4]. The advancements to be made in this paper are solving the governing equations on an adaptive grid system and representing the radiative transfer without making the diffusion approximation.

The plasma hydrodynamics in both ion beam transport channels and ICF target explosions has characteristics of steep gradients and shock structures that need to be handled with a robust computational grid system. In this paper, we describe an adaptive-grid finite difference scheme for ICF plasmas in the frame of radiation hydrodynamics that satisfies this need.

2. ADAPTIVE-GRID SYSTEM

The grid generation is based on the equidistribution principle [5, 6]

$$\Delta x \cdot W(x) = \text{const}$$

which states that at every timestep in the simulations the mesh points are arranged such that this product remains constant. Here, Δx is the cell size and W is a cell-averaged weight function. This principle leads to an explicit grid generation technique that has some advantages over an implicit one. It is easy to apply and easy to control such a mesh distribution. Mesh smoothness is simple and robust. In the present work, the smoothness is done on the weight

0021-9991/92 $5.00

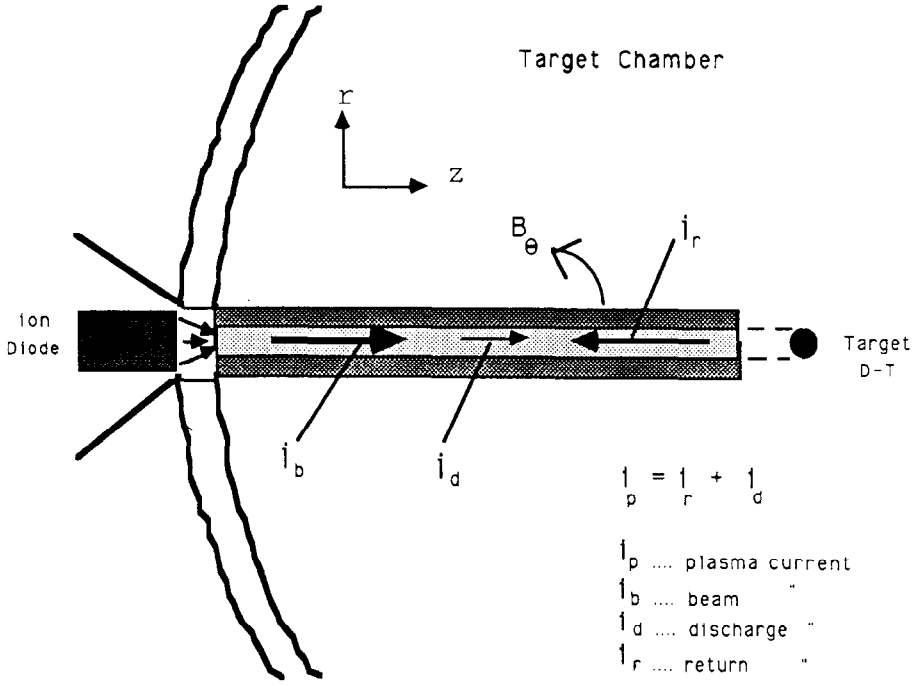

FIG. 1. Schematic of beam propagating plasma channel in LIB fusion.

function W, which indeed results in a smooth grid distribution.

Governing partial differential equations for fluid systems are generally described using a laboratory frame of reference. They can be transformed to a more general reference frame that reduces to the eulerian and lagrangian frames when the reference velocity is zero or equal to the local fluid velocity. In order to transfer the governing equations from (r, t) to an adaptive system (ξ, τ), we use a variable transformation as follows

$$\tau = t$$

$$\xi = \xi(r, t)$$

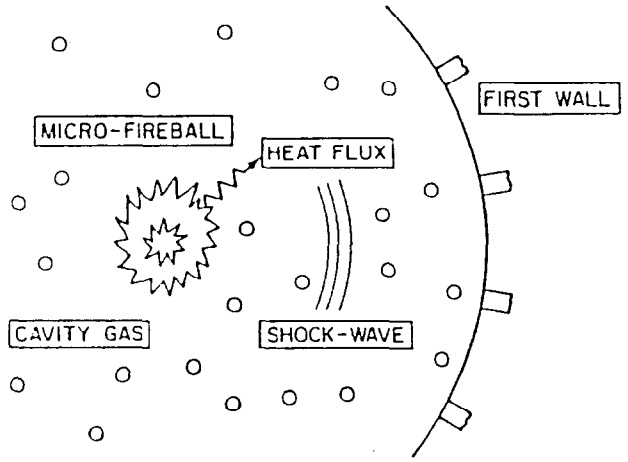

FIG. 2. Schematic diagram showing the physical processes occurring in an ICF target chamber after target explosion [23].

and, thus,

$$\frac{\partial}{\partial \tau} = \frac{\partial}{\partial r}\frac{\partial r}{\partial \tau} + \frac{\partial}{\partial t}\frac{\partial t}{\partial \tau},$$

$$\frac{\partial}{\partial \xi} = \frac{\partial}{\partial r}\frac{\partial r}{\partial \xi} + \frac{\partial}{\partial t}\frac{\partial t}{\partial \xi}.$$

We choose $\partial t/\partial \tau = 1$ and $\partial t/\partial \xi = 0$. That leaves us with

$$\frac{\partial}{\partial t} = \frac{\partial}{\partial \tau} - r_\tau \frac{\partial}{\partial r},$$

$$\frac{\partial}{\partial r} = \frac{1}{r_\xi}\frac{\partial}{\partial \xi}$$

or, in another representation,

$$\begin{aligned} [\ ]_t &= [\ ]_\tau - r_\tau [\ ]_r \\ [\ ]_r &= \frac{1}{r_\xi}[\ ]_\xi. \end{aligned} \tag{1}$$

Here, r_ξ and r_τ are the mesh metric (jacobian) and the speed that will appear with the unknowns in the transformed equations. In order to solve the set of transformed equations, which are given in Section 4, we must estimate these mesh quantities in advance.

The information required about these quantities could be sought for the time t^{n+1} as well as for the time t^n. However, before any attempt to solve physical equations at t^{n+1}, we

let the mesh points move from t^n to t^{n+1} depending on the values and *gradients* of some chosen physical variables at t^n. This procedure of determining the mesh distribution at t^{n+1} in terms of information given at the t^n is an *explicit* procedure. The equidistribution principle and the variable transformation described before leads to the following expression, that can be used in an explicit manner for mesh generation [6],

$$\int_0^x W\,dx' = \xi(x)\left(\frac{\int_0^L W\,dx'}{N}\right). \tag{2}$$

Here $\xi(x)$ is simply a function whose value is chosen to be equal to the mesh number. The second term on the right-hand side represents the average $W\,\Delta x$ for each mesh cell. We call this procedure "explicit" because all the quantities on the right-hand side are given at t^n and the weight function W on the left-hand side is also defined at t^n with the exception of the integral's upper limit x being given at t^{n+1}. After x^{n+1} is calculated, the mesh edge velocity could be found by differencing the old and new values of x with respect to time. The formula for this, x_τ, will be given later in another section. The mesh metric x_ξ is simply the difference in the space locations, equal to Δx if $\Delta\xi$ is taken to be 1.

Therefore, knowing x_ξ and x_τ beforehand, the physical equations can be evaluated without any difficulty. However, one has to determine what the weight function should be. Many forms of weight function can be postulated. One that proves to be both simple and robust is the following

$$W = 1 + \alpha_a |A_x| + \beta_a |A_{xx}| + \alpha_b |B_x| + \beta_b |B_{xx}|, \tag{3}$$

where A and B are some normalized physical quantity such as *velocity*, *pressure*, *mass density*, *momentum density*, or *temperature*. Also A_x, A_{xx}, B_x, and B_{xx} are the first and second derivatives of A and B with respect to the spatial coordinate x. Dwyer [7, 8] has developed a strategy to determine α and β through a specified fraction of points to be assigned to each function variation. That is, if R_α is defined as the fraction of grid points to be assigned to the first derivative variation, U_x, then

$$\alpha \int_0^L |U_x|\,dx = R_\alpha \int_0^L (1 + \alpha |U_x| + \beta |U_{xx}|)\,dx \tag{4}$$

and also for the second degree of variation U_{xx},

$$\beta \int_0^L |U_{xx}|\,dx = R_\beta \int_0^L (1 + \alpha |U_x| + \beta |U_{xx}|)\,dx. \tag{5}$$

If R_α and R_β are held constant for the problem, then α and β will be determined at each time step while the solution develops. Determining α's and β's from these equations follows an explicit procedure that uses the old values at time t^n on the right-hand-side to come up with new values at time t^{n+1} on the left-hand side. In fact, one could time-average the old and new values as we have done. Also, one does need an initial guess, such as the following, to start the procedure:

$$\beta = 0;$$

thus from Eq. (4),

$$\alpha = \frac{R_\alpha L}{(1 - R_\alpha)\int_0^L |U_x|\,dx}. \tag{6}$$

Thus, R is the fraction of mesh points that are reserved for chosen gradients of A or B. Notice that Eq. (3) enables one to construct W out of two variables, A and B, which means one can *adapt* using more than one function. This obviously enhances the power of solving *multigradient* problems accurately.

3. RADIATION-MAGNETOHYDRODYNAMICS

We analyze only the radial motion of the plasma and thus assume a one-dimensional model symmetry in all other dimensions. The equations are presented for curvilinear as well as cartesian coordinates. The problem of ion beam transport channels is in cylindrical geometry as shown in Fig. 1 whereas the target explosion problem is studied in spherical geometry, shown in Fig. 2. The radiation hydrodynamics equations are written in the laboratory frame and then transferred to the adaptive grid frame. They are solved along with a set of grid equations, based on Eq. (2), that describes how the grid system evolves in time. The explicit grid generation procedure prevents implicit coupling between the physical equations and the grid system. A conservative differencing scheme based on the control volume approach is chosen to retain the conservative nature of the governing equations. The numerical method to discretize the equations is a first-order upwind differencing scheme (donor cell). The dissipative characteristics of the upwind differencing are minimized with grid adaptation.

The governing equations for a nonrelativistic fluid in the frame of radiation-magnetohydrodynamics (R-MHD) are described as [9, 10]

$$\frac{\partial \rho}{\partial t} + \nabla\cdot(\rho\mathbf{u}) = 0$$

$$\frac{\partial}{\partial t}\left(\rho\mathbf{u} + \frac{1}{c^2}\mathbf{F}\right) + \nabla p + \nabla\cdot(\rho\mathbf{u}\mathbf{u} + \vec{\mathbf{P}}) = \frac{\mathbf{J}\times\mathbf{B}}{c} \tag{7}$$

$$\frac{\partial}{\partial t}(e_p + e_R) + \nabla\cdot(\mathbf{q} + (e_p + p)\mathbf{u} + \mathbf{F}) = \mathbf{J}\cdot\mathbf{E}$$

where e_p and e_R are energy density for plasma and radiation, $\mathbf{F}$ and $\vec{\mathbf{P}}$ are radiation flux and pressure tensor. Also $\mathbf{J}\cdot\mathbf{E}$ is the Joule heating term and is equal to $\mathbf{E}'\cdot\mathbf{J}'$, the rate of Joulean dissipation in fluid frame, plus $\mathbf{u}\cdot(\mathbf{J}\times\mathbf{B}/c)$, the rate at which the force $\mathbf{J}\times\mathbf{B}/c$ does work. A relation is needed between the pressure, density, and temperature to close the system. This relation can be found using the equation of state

$$p=(1+\bar{Z})\,nkT,$$

where $\bar{Z}$ is the average charge state, n is number density, and T is temperature.

The state of the radiation field and the magnetic field are found through the radiative transfer equation, the Maxwell's equations and Ohm's law, respectively. The radiative transfer equation is a mathematical statement of the conservation of photons and is given in the form [11]

$$\left(\frac{1}{c}\frac{\partial}{\partial t}+\hat{\Omega}\cdot\nabla\right)I(\mathbf{r},t,\hat{\Omega},\nu)=\eta(\mathbf{r},t,\hat{\Omega},\nu)-\chi(\mathbf{r},t,\hat{\Omega},\nu)\,I(\mathbf{r},t,\hat{\Omega},\nu), \tag{8}$$

where I is specific intensity, η and χ are called emissivity and extinction coefficients, and $\hat{\Omega}$ is the directional unit vector. The space-time evolution of the magnetic field in the MHD approximation is given as

$$\frac{\partial\mathbf{B}}{\partial t}=\nabla\times(\mathbf{u}\times\mathbf{B})-\nabla\times\left(\frac{c^2}{4\pi\sigma}\nabla\times\mathbf{B}\right), \tag{9}$$

where σ is the electrical conductivity of the plasma. The equation describes how the magnetic field lines are convected and diffused in the non-relativistic and low-frequency plasma fluid.

In cylindrical coordinates, particularly for the z-pinch plasma problem, the radial dependence of an azimuthal magnetic field interacting with an axial current becomes

$$\frac{1}{c}\frac{\partial B}{\partial t}-\frac{\partial}{\partial r}\left(\frac{\eta c}{4\pi}\frac{1}{r}\frac{\partial}{\partial r}(rB)\right)+\frac{1}{c}\frac{\partial}{\partial r}(uB)=-\frac{\partial}{\partial r}(\eta J_b). \tag{10}$$

Here J_b is the ion beam current density flowing in the channel, and η is the plasma resistivity. Also the multigroup photon conservation equation in one-dimensional (radial) cylindrical coordinates becomes

$$\frac{1}{c}\frac{\partial}{\partial t}I_g(r,t,\hat{\Omega})+\frac{\mu}{r}\frac{\partial}{\partial r}(rI_g(r,t,\hat{\Omega}))-\frac{1}{r}\frac{\partial}{\partial\omega}(\zeta I_g(r,t,\hat{\Omega}))=\eta_g-\bar{\chi}_g I_g(r,t,\hat{\Omega}), \tag{11}$$

where we have replaced the streaming term [12] in the radiative transfer equation by

$$\hat{\Omega}\cdot\nabla I_g=\frac{\mu}{r}\frac{\partial}{\partial r}(rI_g)-\frac{1}{r}\frac{\partial}{\partial\omega}(\zeta I_g). \tag{12}$$

The group constants η_g and $\bar{\chi}_g$ are given as

$$\eta_g=\int_{\nu_{g-1}}^{\nu_g}\eta_\nu\,d\nu$$

and

$$\bar{\chi}_g=\frac{\int_{\nu_{g-1}}^{\nu_g}\chi\,d\nu}{\int_{\nu_{g-1}}^{\nu_g}d\nu}, \tag{13}$$

assuming that one has enough groups so that χ is nearly constant for each group. All radiation and material properties on the RHS of Eq. (8), (11), and (13) are being measured in the inertial (lab) frame and they are assumed to be isotropic. Actually, there is a need to account for the velocity-dependence of these terms but this velocity-dependence is on the order of $O(v/c)$ and the authors believe the velocity-induced frequency shifts are ignorable for the problems of interest. The alternative is to use radiation/material properties evaluated in the comoving frame [11]. Here μ, ω, and ζ are angular variables as shown in Fig. 3. Cylindrical coordinates are complicated by the fact that even in one spatial dimension two angular variables, ζ and ω, are needed to describe the angular dependency of specific

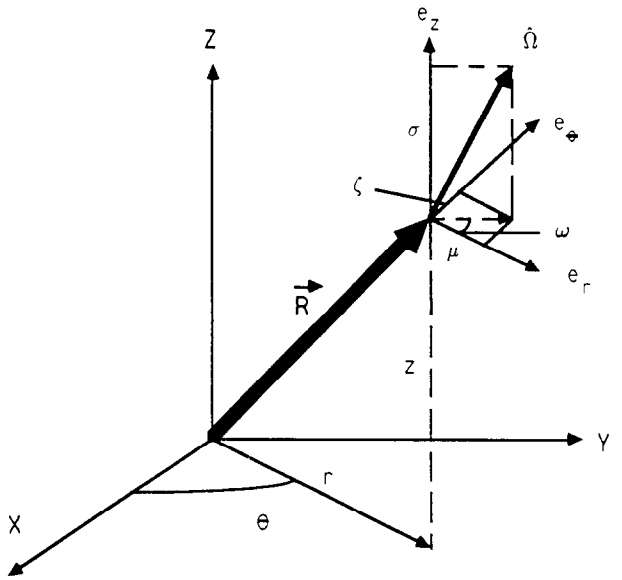

FIG. 3. Cylindrical space-angle coordinate system.

intensity I. As shown in Fig. 3, ω is the angle between $\hat{r}$ and $\hat{\Omega}$, and thus

$$\mu = (1-\sigma^2)^{1/2}\cos\omega$$
$$\zeta = (1-\sigma^2)^{1/2}\sin\omega. \tag{14}$$

The angular discretization can be done with a level-symmetric quadrature set described in [12, 16].

4. EQUATIONS ON ADAPTIVE GRID SYSTEM

Transforming the R-MHD equations, Eq. (7), to the adaptive frame, we reach the following one-dimensional adaptive fluid equations:

Continuity:

$$[x_\xi x^\delta \rho]_\tau + [x^\delta \rho(u - x_\tau)]_\xi = 0,$$

Momentum:

$$[x_\xi x^\delta(\rho u + c^{-2}F)]_\tau + [x^\delta \rho u(u - x_\tau)]_\xi - [x^\delta x_\tau c^{-2}F]_\xi + x^\delta[p]_\xi + [x^\delta P]_\xi = x^\delta x_\xi F_m,$$

Energy:

$$[x_\xi x^\delta(e_p + e_R)]_\tau + [x^\delta e_p(u - x_\tau)]_\xi - [x^\delta x_\tau e_R]_\xi + [x^\delta(pu + q + F)]_\xi = x^\delta x_\xi E_m, \tag{15}$$

where $\delta = 0, 1, 2$ for *planar*, *cylindrical*, and *spherical* coordinates. Here F_m and E_m are the electromagnetic force and energy for the chosen coordinate system.

It is important to recognize that for curvilinear geometries the identity

$$[x^\delta x_\xi]_\tau = [x^\delta x_\tau]_\xi$$

must be preserved in the difference equations in order for them to preserve the conservative form as in Eq. (15). That is, when differenced equations are solved on the discretized coordinates, care should be taken to provide this identity relation which also introduces a formula to calculate the grid speed while the grid points move from x^n to x^{n+1}. This formula will be given in the next section.

5. DISCRETIZATION

There are two paths to discretize the given equations: the differential approach and the control volume approach. In the differential approach, the equations are considered to be PDEs and it follows a pure mathematical track, and the physical significance of the variables can be lost. In the control volume approach, the conservative nature of the equations is preserved. For our adaptive mesh scheme, the control volume approach is the only viable approach if conservation of the physical quantities is to be achieved [6]. The reason is that the mesh dilates and translates during each time step, thus the relative fluid and mesh velocities at the cell edges and at the center are different. Care should be given to distinguish the cell edge and center velocities, which is done in the control volume approach. Most control volume schemes define the location of *density*, *pressure*, and *energy* at the center of the mesh while defining the location of the velocities at the mesh edge as shown in Fig. 4.

Under the control volume approach, the *identity* equation

$$[x^\delta x_\xi]_\tau = [x^\delta x_\tau]_\xi$$

is discretized as

$$\frac{(x^\delta x_\xi)_i^{n+1} - (x^\delta x_\xi)_i^n}{\Delta\tau} = (x^\delta x_\tau)_{i+1/2}^n - (x^\delta x_\tau)_{i-1/2}^n,$$

where indices i and $i \mp \frac{1}{2}$ represent the ith cell's center and edge values. ξ is chosen to be the successive number of mesh points as explained in Section 2. Therefore $\Delta\xi$ is equal to 1. For this difference equation to conserve the involved quantities, the cell edge velocities should be given as

$$(x_\tau)_{i\mp 1/2}^n = \frac{(x^\delta)_i^{n+1} x_{i\mp 1/2}^{n+1} - x_{i\mp 1/2}^n (x^\delta)_i^n}{(x^\delta)_{i\mp 1/2}^n \Delta\tau}. \tag{16}$$

Before discretizing the fluid equations in Eq. (15), we introduce a *von Neumann–Richtmyer* artificial viscosity [13] that replaces the fluid pressure by

$$p \Rightarrow p + Q,$$

where $Q = -\rho(C\,\Delta x)^2\,|\Delta u/\Delta x|\,\Delta u/\Delta x$. Here C is the artifi-

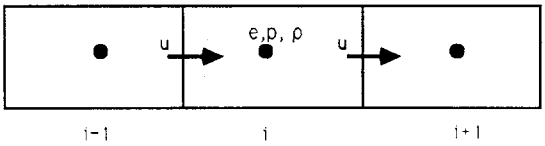

a) Cell edge oriented

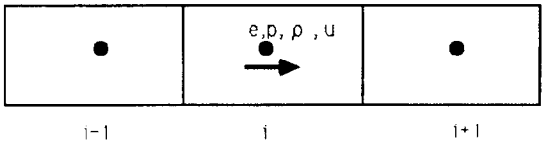

b) Cell center oriented

FIG. 4. Control volume approach.

cial viscosity model coefficient and u is the fluid velocity. Although the inclusion of such numerical dissipation may not be necessary with an already dissipative upwind differencing, we have kept it there to test its effects and, for the simulations in this paper, C is 1.

The fluid equations are then discretized as follows:

Continuity equation. $[x^\delta x_\xi \rho]_\tau + [x^\delta \rho(u - x_\tau)]_\xi = 0$. An explicit control volume scheme gives

$$\frac{(x^\delta x_\xi \rho)_i^{n+1} - (x^\delta x_\xi \rho)_i^n}{\Delta\tau} + \frac{(x^\delta \rho(u - x_\tau))_{i+1/2}^n - (x^\delta \rho(u - x_\tau))_{i-1/2}^n}{\Delta\xi} = 0.$$

Because ξ is under our control we choose it to be the number of mesh points, say $\xi = 1$ for the first mesh point and 2, 3, ..., N for the rest. From this, $\Delta\xi$ becomes unity ($\Delta x_i = 1$). In order to evaluate the cell edge ($i \mp \frac{1}{2}$) values of physical variables we apply a first-order *upwind* (donor cell) scheme [14]. This scheme simply equates the edge value with one of the neighboring cell center values depending upon the sign of the edge velocity $u_{i \mp 1/2}$. That is,

$$\rho_{i+1/2} = \rho_i \quad \text{if} \quad u_{i+1/2} \geq 0$$

and

$$\rho_{i+1/2} = \rho_{i+1} \quad \text{if} \quad u_{i+1/2} < 0$$

and

$$\rho_{i-1/2} = \rho_{i-1} \quad \text{if} \quad u_{i-1/2} \geq 0$$

and

$$\rho_{i-1/2} = \rho_i \quad \text{if} \quad u_{i-1/2} < 0.$$

The differencing formula to find ρ_i^{n+1} is then

$$\rho_i^{n+1} = \frac{1}{(x^\delta x_\xi)_i^{n+1}} \{(x^\delta x_\xi \rho)_i^n - \Delta\tau \{(x^\delta \rho(u - x_\tau))_{i+1/2}^n - (x^\delta \rho(u - x_\tau))_{i-1/2}^n\}\}. \tag{17}$$

Note that the mesh distribution $(x^\delta, x_\xi, x_\tau)$ on the right-hand side at time t^n and t^{n+1} is known before the partial differential equation is solved for ρ_i^{n+1}. The method of determining the mesh distribution was discussed earlier in Section 2.

Momentum equation. The same discussion for the continuity equation applies for the momentum equation except that the discretization on the pressure term is not done by the upwind scheme, but rather is [14]

$$[p]_\xi = \frac{p_{i+1} - p_{i-1}}{\Delta\xi_i + \Delta\xi_{i-1}} = \frac{p_{i+1} - p_{i-1}}{2}.$$

The differenced momentum equation for the radiating-magnetized plasma is then

$$\begin{aligned}
&\frac{1}{\Delta\tau}\left\{\left(x^\delta x_\xi\left(\rho u + \frac{F}{c^2}\right)\right)_i^{n+1} - \left(x^\delta x_\xi\left(\rho u + \frac{F}{c^2}\right)\right)_i^n\right\} \\
&\quad + \{(x^\delta \rho u(u - x_\tau))_{i+1/2}^n - (x^\delta \rho u(u - x_\tau))_{i-1/2}^n\} \\
&\quad - \left\{\left(x^\delta x_\tau \frac{F}{c^2}\right)_{i+1/2}^n - \left(x^\delta x_\tau \frac{F}{c^2}\right)_{i-1/2}^n\right\} \\
&\quad + x_i^\delta\left(\left\{\frac{p_{i+1}^n - p_{i-1}^n}{2}\right\} + \left\{\frac{P_{i+1}^n - P_{i-1}^n}{2}\right\}\right) \\
&\quad - (x^\delta x_\xi)_i^n F_m = 0.
\end{aligned} \tag{18}$$

Again, the upwind scheme is used to evaluate the cell edge values. As a last step u_i^{n+1} is found provided that all values at time t^n, and F at time t^{n+1}, are known. Ideally, the plasma equations and the auxiliary radiation field equation are to be solved simultaneously, but because of the explicit scheme being used here, one can solve the radiation field for t^{n+1} upon plasma properties at t^n and then further solve the plasma equations. The magnetic force F_m in the fluid equation appears to be at t^n, therefore $(F_m)_i^n$ is known in advance.

Energy equation. Recall that the energy equation for the radiating-magnetized plasma is

$$[x^\delta x_\xi(e_p + e_R)]_\tau + [x^\delta e_p(u - x_\tau)]_\xi - [x^\delta x_\tau e_R]_\xi + [x^\delta pu]_\xi + [x^\delta(q + F)]_\xi - x^\delta x_\xi E_m = 0.$$

The differenced form is

$$\begin{aligned}
&\frac{1}{\Delta\tau}\{(x^\delta x_\xi(e_p + e_R))_i^{n+1} - (x^\delta x_\xi(e_p + e_R))_i^n\} \\
&\quad + \{(x^\delta e_p(u - x_\tau))_{i+1/2}^n - (x^\delta e_p(u - x_\tau))_{i-1/2}^n\} \\
&\quad - \{(x^\delta x_\tau e_R)_{i+1/2}^n - (x^\delta x_\tau e_R)_{i-1/2}^n\} \\
&\quad + \{(x^\delta pu)_{i+1/2}^n - (x^\delta pu)_{i-1/2}^n\} \\
&\quad + \{(x^\delta(q + F))_{i+1/2}^n - (x^\delta(q + F)_{i-1/2}^n\} \\
&\quad - (x^\delta x_\xi)_i^n (E_m)_i^n = 0.
\end{aligned} \tag{19}$$

This equation is solved for $(e_p)_i^{n+1}$ in terms of the values given partially at time t^n and at time t^{n+1} (x_ξ, x_τ, e_R).

6. APPLICATIONS

Two applications are chosen to demonstrate the adaptive hydrodynamics scheme. The first examines how the grid redistribution handles severe discontinuities. In the second, we compare our plasma channel simulations with those found by a lagrangian multigroup radiation diffusion scheme. A list of the major steps that our numerical procedure follows to update the equations on an adaptive mesh from time t^n to t^{n+1} is given below:

- Given the fraction of the mesh points to be used for the first and second degree variation of the chosen adaptive function, R_α and R_β, calculate α and β through Eqs. (4) and (5).
- Calculate the weight function w using updated values (time t^n) of the chosen adaptive function.
- Compute new mesh points, x_ξ and mesh speeds, x_τ by Eqs. (2) and (16).
- Solve the governing equations for time t^{n+1}.
- Set up the new time step.
- Repeat steps.

Time step control is done by fixing the CFL number globally. The compressible flow CFL number is typically defined [14] for a fixed mesh system as

$$CFL = (|u| + a)\frac{\Delta t}{\Delta x},$$

where a is the local sound speed. For an adaptive scheme we can define the CFL number as

$$CFL = (|u_{\text{cell}}| + a)\frac{\Delta t}{\Delta x},$$

where $u_{\text{cell}} = \frac{1}{2}(u_r + u_l)$, u_r and u_l being the right and left edge velocities.

6.1. *Shock Tube*

A common benchmark problem for new CFD models is the *shock tube* problem by which the method is examined against severe discontinuities. Hence, the following section will present how our adaptive mesh scheme treats such a problem. The magnetic and radiative properties of the fluid are artificially ignored, assuming a pure gas dynamical flow. An analytic solution to this problem (Sod's shock tube [15]) does exist for comparison with the numerical hydrodynamics calculations. The problem is studied here in only one spatial dimension and in one geometry (planar), although its applications in curvilinear geometries are studied elsewhere by the authors [16]. The physical domain is divided into two regions of different conditions as

$$\begin{aligned} \textit{Left} \quad & P_L = 1.0,\ \rho_L = 1.0,\ e_L = 2.5, \\ & u_L = 0,\ 0.0 \leqslant x \leqslant 0.5, \\ \textit{Right} \quad & P_R = 0.1,\ \rho_R = 0.125,\ e_R = 2.0, \\ & u_R = 0,\ 0.5 \leqslant x \leqslant 1.0, \end{aligned} \tag{20}$$

Here, also the ideal gas equation of state,

$$P = (\gamma - 1)\, e\rho; \quad \gamma = 1.4, \tag{21}$$

is assumed and the boundary conditions at $x = 0$ and $x = 1$ are reflective. A complete history of the time evolution of the problem, even up to the late times where no analytical solution exists, is given by Winkler *et al.* [17, 18], and this is taken as a reference for comparison.

The region L has higher pressure and thus higher density. At time $t = 0^+$ the system is released and a shock front is formed, propagating to the right. In a shock problem like this there are three distinct regions that must be resolved by the numerical method: (1) the shock wave, (2) the contact discontinuity, and (3) the rarefaction wave. The simulations are done over 100 mesh points with the adaptation functions being the *momentum density* with $R_\alpha = 0.35$ and $R_\beta = 0.15$ and the CFL number being 0.5. Figure 5 shows the mass density profiles for $t = 0.01079$, 0.228, 0.364, and 1 s with no adaptation at all (fixed mesh system). Besides

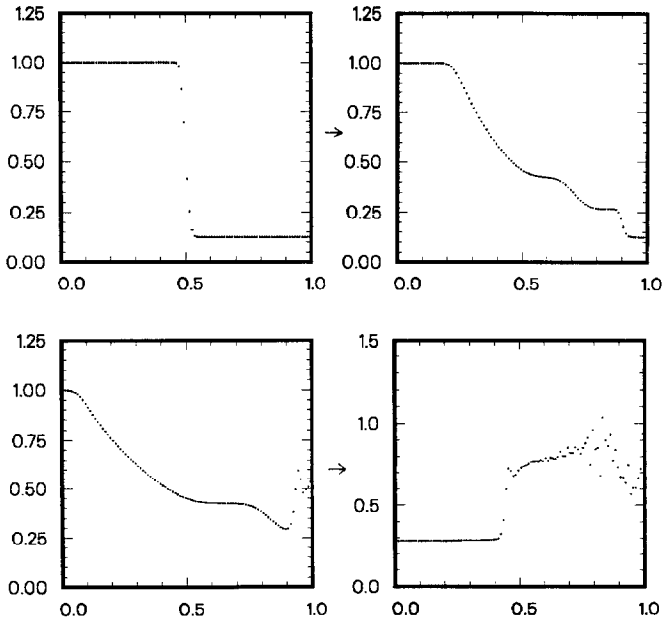

FIG. 5. Mass density of Sod's shock-tube problem at times $t = 0.001079$, 0.228, 0.364, and 1.0 with no adaptation. Grid points are shown individually.

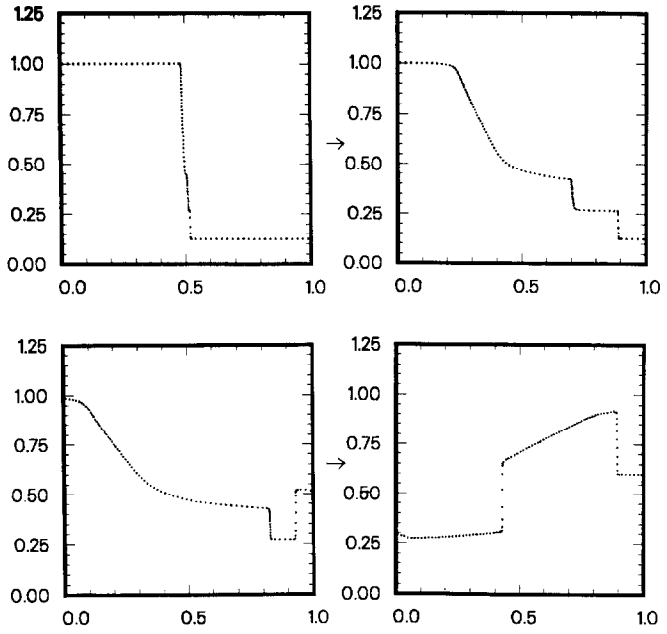

FIG. 6. Mass density of Sod's shock-tube problem at times $t = 0.01079$, 0.228, 0.364, and 1.0 with adaptation. Grid points are shown individually.

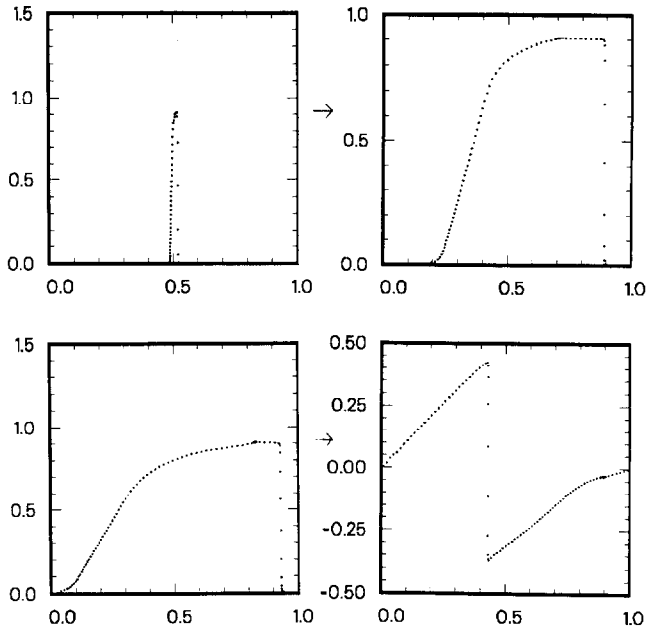

FIG. 8. Velocity profiles of Sod's shock-tube problem at times $t = 0.01079$, 0.228, 0.364, and 1.0 with adaptation. Grid points are shown individually.

the characteristics of the eulerian grid scheme, these results reflect those of the first-order upwind scheme used in the model. These results are similar to those by Sod [15] for an upwind difference scheme, except that we do not see any artificial shock which Sod describes to be between the left constant state and the left endpoint of the rarefaction wave. However, as reported by Sod, the upwind differencing on a fixed grid system is not very satisfactory. The corners at the endpoints of the rarefaction, the discontinuity, and the shock are extremely rounded, showing how diffusive the numerical scheme is. Also the reflection from the wall and the interaction of waves after the reflection is

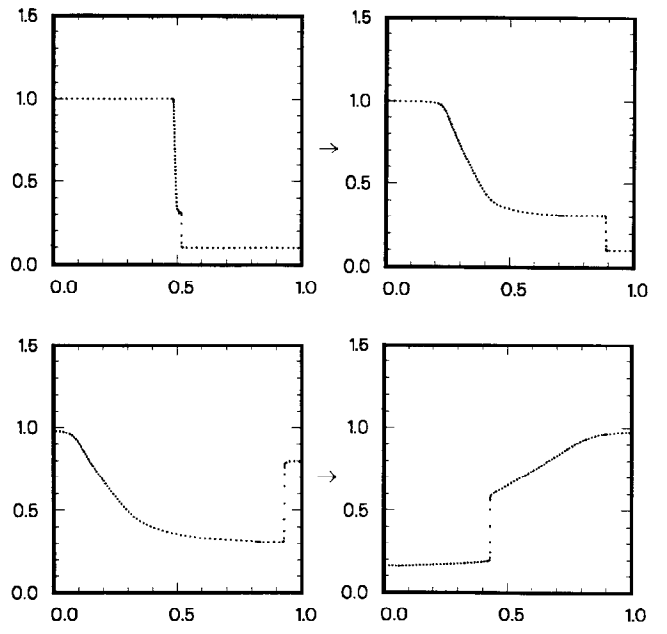

FIG. 7. Pressure profiles of Sod's shock-tube problem at times $t = 0.01079$, 0.228, 0.364, and 1.0 with adaptation. Grid points are shown individually.

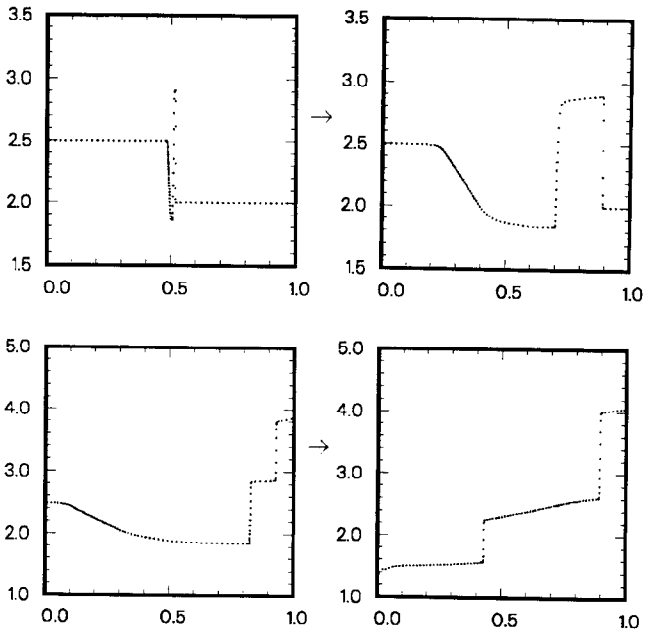

FIG. 9. Internal energy profiles of Sod's shock-tube problem at times $t = 0.01079$, 0.228, 0.364, and 1.0 with adaptation. Grid points are shown individually.

misrepresented by the numerical oscillations, where using an adaptive grid system can be utilized most.

Figures 6, 7, 8, and 9 show the mass density, pressure, velocity, and internal energy profiles for the same problem using an explicit adaptive mesh. The resolution at the corners clearly point to the advantage of using the adaptive scheme. Adapting the mass density seems to be capturing most of the steep gradients in pressure, velocity, and internal energy, too. The mesh spacing is inherently limited to some degree in our explicit adaptive scheme since the stability criteria requires smaller timesteps for finer mesh spacing. Note how the adaptive mesh counteracted the diffusive nature of a first-order scheme (upwind differencing). The diffusive characteristic of the upwind scheme may still be seen around the rarefaction region and this warrants future investigation into second-order schemes. When compared to Winkler's results in Fig. 10, our results show a very good agreement. The location of the shock front and the contact discontinuity, the reflection from the boundary all indicate the scheme's robustness, except that its resolution power is not as impressive as Winkler's implicit adaptive grid method. The advantages and disadvantages of implicit and explicit schemes, however, still make both methods equally interesting.

6.2. *Dynamics of Z-Pinch Plasma Channels*

Lagrangian grid schemes have often been used to model this type of problem. Typical plasma channel simulations by ZPINCH [3] indicate a blast wave character of the discharge plasma while it is interacting with the magnetic field. The nature of the z-discharge plasma channel problem creates steep gradients in density, temperature, and electrical conductivity which one would like to resolve. Being a lagrangian code, ZPINCH automatically resolves only density gradients, yet because the density is low in the region where the temperature (and hence the conductivity) peaks, the mesh in this region is elongated. This effect tends to smear the temperature and magnetic field gradients in space, thus losing the resolution (accuracy) needed to follow this non-linear conduction problem.

The weakness of the ZPINCH code is not only the grid

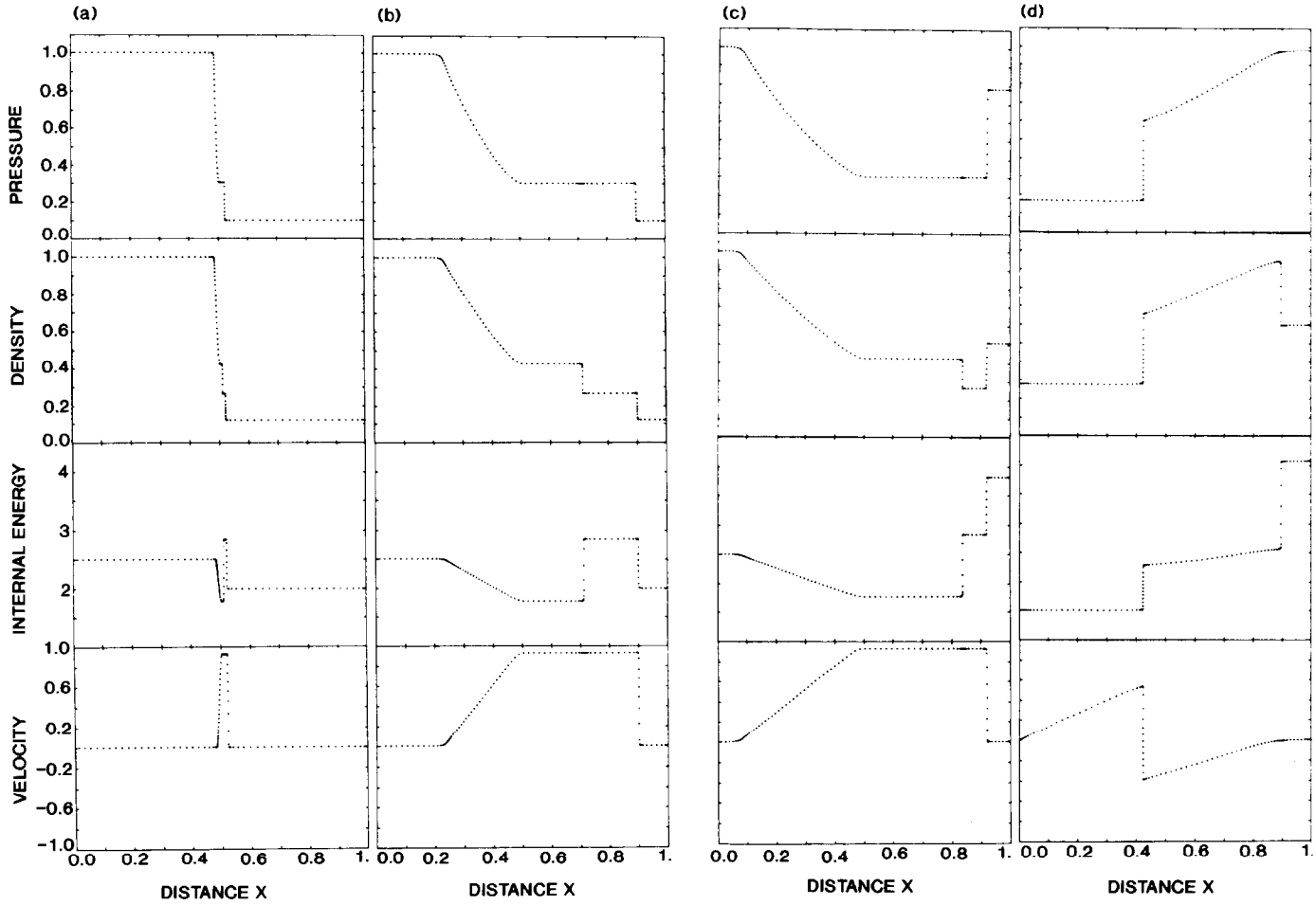

FIG. 10. Numerical solution of Sod's shock-tube test problem by Winkler *et al.* [17] at times $t = 0.01079, 0.228, 0.364$, and 1.0. Grid points are shown individually.

system. It also treats the radiation in the channel with a diffusion approximation, despite the fact that the mean free path of X rays in most of the plasmas (argon, helium) used for z-pinch channels is much larger than the physical dimensions of the channel. Hence, the diffusion approximation of radiation hydrodynamics is simply inadequate for such applications. To show what we have gained by developing an adaptive-grid radiative transfer scheme, namely R-MHD, as opposed to a lagrangian scheme for ICF plasmas, we will present a comparison of our plasma channel results with those by ZPINCH. The channel is a cylindrical column filled with argon gas of initially uniform density 2.32×10^{-5} g/cm^3. The supplementary data (equation of state and opacity tables) were taken from an atomic physics code [22] which treats non-LTE plasma conditions. The simulations assumed an argon gas with an initial gaussian temperature profile corresponding to heating by a preionizing laser beam of 2 mm half-width. Simulations are done in three approximations: pure hydrodynamics (HD), magnetohydrodynamics (MHD), and radiation-magneto-hydrodynamics (R-MHD), meaning that we artificially turned off the discharge current and the radiation field to check various effects in each case.

We have tried different adaptation functions (i.e., temperature, resistivity, momentum, momentum-resistivity, and momentum-temperature) and noted the importance of the adaptation in such calculations. Due to the fact that a momentum density (ρw) adaptation keeps the point concentration high all over the inner region of the channel, we have done the final simulation with that adaptation. The number of mesh points is 50, all spread in a channel of 1-cm radius. The user-defined R_α and R_β constants are 0.3 and 0.1, respectively. The number of frequency groups was chosen to be 20, and the angular discretization is based on a S-6 level-symmetric quadratic discrete ordinates set as described in detail in Ref. [16].

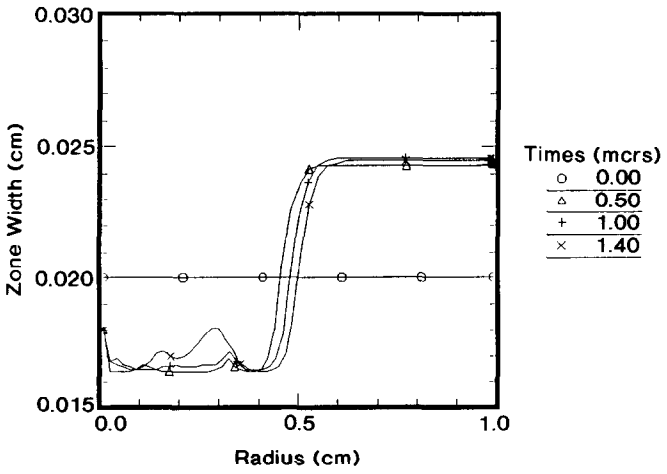

FIG. 11. Adaptive mesh distribution at various times.

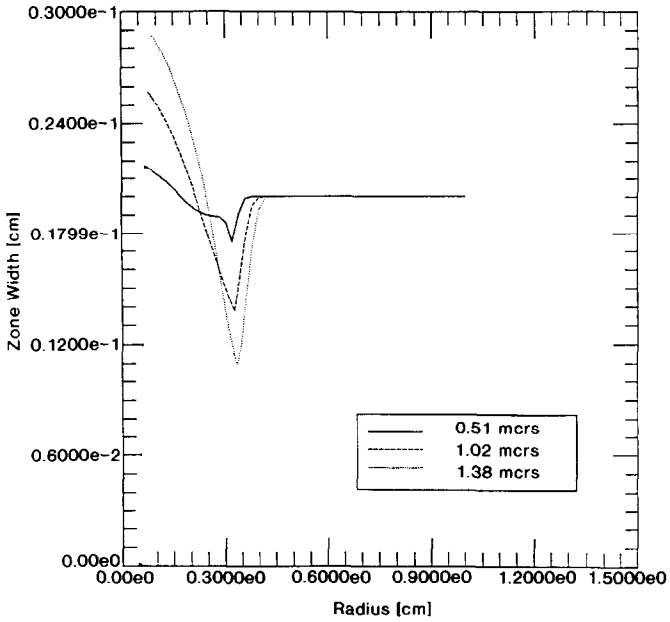

FIG. 12. Lagrangian mesh distribution at various times.

For the pure hydrodynamic case the mesh distribution for the lagrangian grid and the adaptive grid is shown in Fig. 11 and 12. Figures 13 and 14 show the density profiles, and also Table I compares the mesh spacing for both grid schemes. As mentioned before, lagrangian zones concentrate where the density peak lies; thus they leave few points at the center (rarefaction) region, where a finer mesh distribution is needed when the magnetic and radiation fields are included. Note that the lagrangian scheme has put a lot of points around the density peak, and the mesh spacing it provides at that point is better than ours, although we could achieve this too by adjusting our user-given R_α and R_β, or by changing the adaptation function. The adaptation scheme, on the other hand, adapted the points on the momentum density, which has a relatively mild gradient starting from the channel center to the density peak point. Thus it distributes the points with a balanced manner in the inner channel providing a platform for possible multi-gradients in temperature and magnetic field. The outcome of Fig. 11 through 14 and Table I is that the lagrangian grid may be good enough for pure hydrodynamics cases, since there are no interesting gradients behind the density peak where actually the adaptive scheme provides a finer mesh

TABLE I

Mesh Spacing at Various Points at Time 1.4 μs

Method	Δx at $r = 0$	Δx at density peak	$\overline{\Delta x}$
R-MHD	0.0165	0.016	0.017
ZPINCH	0.0287	0.011	0.021

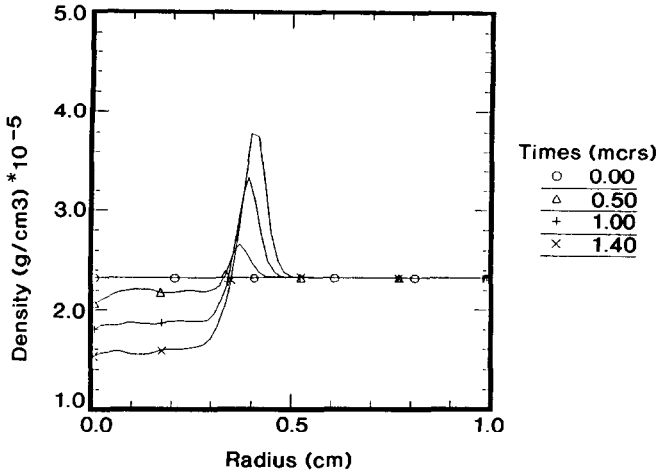

FIG. 13. Mass density profiles (R-MHD) at various times.

spacing. However, we should recall the fact that finer mesh spacing does increase the accuracy, and clearly here the average mesh spacing gained with the adaptive scheme throughout the channel is better than that of the lagrangian.

The effect of radiation on the channel dynamics can be observed by comparing Tables II and III. The results (peak magnetic field B_c and the corresponding channel radius r_c, channel-center temperature T_0) are very different between the ZPINCH and R-MHD. With the introduction of radiation in the channel simulation, the change in B_c and r_c is predicted to be 30% by ZPINCH and 10% by R-MHD. ZPINCH indicates further channel expansion, lower magnetic field, and higher energy loss through radiation transfer. The cause for this difference can be classified to be both physical (radiation transport) and numerical

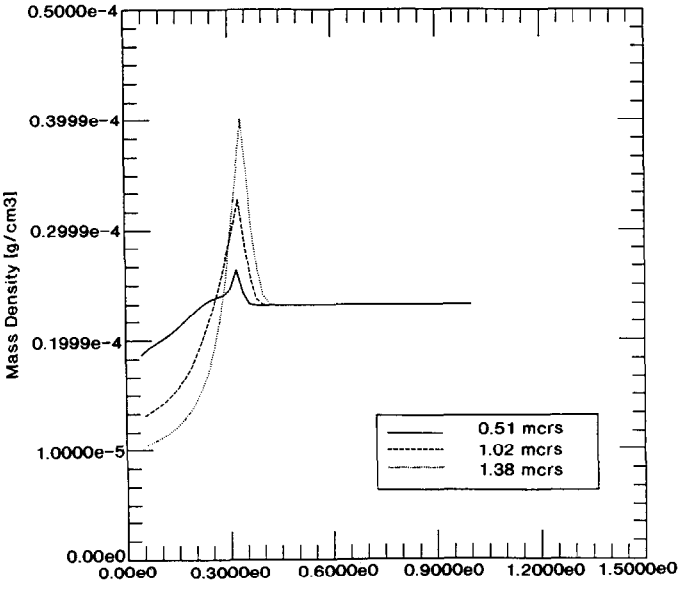

FIG. 14. Mass density profiles (ZPINCH) at various times.

TABLE II

Various MHD Channel Parameters at Time 1.4 μs

Method	Channel radius r_c (cm)	Magnetic field at $r = r_c$ (kG)	$\overline{\Delta x}$ (cm)	Temperature at $r = 0$ (eV)
R-MHD	0.53	22	0.018	11.5
ZPINCH	0.63	18.6	0.030	10

(grid scheme, spatial differencing). Although the difference in radiation transport schemes contributes more to the overall picture, the numerics, as seen in the HD and MHD cases, also plays a role. The peak magnetic field and the corresponding radius between R-MHD and ZPINCH differ around 15% in the MHD case, where the difference is only in numerics, and 35% in the R-MHD case, where the difference is in both numerics and physical modelling. The magnetic field and its channel radius are related as $B_c \propto 1/r_c$; thus a change in one automatically affects the other. Recall that the diffusion model assumes high absorption, and this absorption causes the radiation emitted from central regions to be absorbed at the channel edge. The channel boundary then expands due to the heating and this can further cause a degradation in the magnetic field. If, in fact, the absorption is not that high, then the photons would travel a large distance before being absorbed, and this large distance may actually reside outside the channel. The streaming conditions of photon flux would have to be studied in more detail to solve the frequency- and angular-dependent flux. Doing this and also introducing a more powerful grid scheme, our adaptive-grid radiation-magnetohydrodynamics model has a lot of potential for the study of ICF target explosions and z-pinch plasma channels. Its impact on plasma channel designs has been significant. Earlier studies [24] of different cavity gases (argon, nitrogen, helium) for the LIBRA reactor study indicated that lower atomic number gases (helium) were most suitable for plasma channel formation. We found unacceptable channel spreading due to radiative transfer with the multigroup diffusion approach. Our new set of simulations with the newly developed R-MHD [25] code showed lower absorption and emission by these optically thin gases. Thus,

TABLE III

Various R-MHD Channel Parameters at Time 1.4 μs

Method	Channel radius r_c (cm)	Magnetic field at $r = r_c$ (kG)	$\overline{\Delta x}$ (cm)	Temperature at $r = 0$ (eV)
R-MHD	0.6	19	0.018	5.2
ZPINCH	0.9	12.5	0.020	2.4

application of the new scheme to the LIBRA reactor design indicated the feasibility of high atomic number gases (argon, nitrogen) [26]. Higher atomic number gases are preferable in the cavity for their attenuation of the X rays coming from the target explosion.

7. SUMMARY

The nature of ICF target explosions and beam transport channels create steep gradients in many physical quantities. Lagrangian grid schemes automatically resolve only density gradients, yet because the density is low where other quantities (i.e., temperature) peak, the mesh in this region will be elongated. This effect will tend to smear whatever gradient occurs there, thus causing a lack of resolution needed to follow such non-linear problems. The explicit adaptation scheme based on the equidistribution principle is easily applied to solve hyperbolic conservation laws in one dimension. The first-order upwind finite difference scheme has survived Sod's shock tube problem with the help of the grid adaptation. A local grid refinement factor of 10^2 was found compared to a fixed mesh distribution. Finer mesh spacing would require smaller time-steps and thus a higher cost. When compared to a lagrangian radiation diffusion calculation of plasma channels, our method brings finer grid refinement (a factor of 2) and more accurate description of the radiative transfer in the channel. Applications to z-pinch plasma channels made an impact on the LIBRA channel designs by showing the feasibility of high atomic number (argon, nitrogen) gases for the cavity. The applications to ICF target explosions are also expected to utilize the new model in the near future. The issue of using a second-order accurate method should be considered next in taking the study further. Improvements in plasma modelling include separate electron and ion temperatures. The ion and electron temperature coupling time constant, which depends on the specific heat ratio, may very well be longer than some characteristic timescales in the system. In conclusion, the use of an explicit adaptive grid system has proven to be quite useful and multi-gradient problems are the best candidates to utilize it.

ACKNOWLEDGMENT

Computer time for this research was supplied through a grant from the NSF-sponsored San Diego Supercomputer Center.

REFERENCES

1. G. Yonas, *Bull. Am. Phys. Soc.* **21**, 1102 (1972).
2. R. R. Peterson, University of Wisconsin Fusion Technology Institute Report UWFDM-670, April 1986 (unpublished).
3. J. J. Watrous, G. A. Moses, and R. R. Peterson, University of Wisconsin Fusion Engineering Program Report UWFDM-584, June 1984 (unpublished).
4. R. R. Peterson and G. A. Moses, *Comput. Phys. Commun.* **28**, 405 (1983).
5. J. F. Thompson, Z. U. A. Warsi, and C. W. Mastin, *Numerical Grid Generation* (North-Holland, Amsterdam, 1985).
6. T. J. Bartel, Ph.D. thesis, University of Wisconsin Fusion Engineering Program Report UWFDM-720, Jan. 1987 (unpublished).
7. H. A. Dwyer, *AIAA J.* **22**, No. 12, 1705 (1984).
8. H. A. Dwyer, "A Discussion of Some Criteria for Use of Adaptive Gridding," in *Adaptive Computational Methods For Partial Differential Equations*, edited by I. Babuska (SIAM, Philadelphia, 1983).
9. G. C. Pomraning, *The Equations of Radiation Hydrodynamics* (Pergamon, Elmsford, NY, 1973), p. 220.
10. W. F. Hughes and F. J. Young, *The Electromagnetodynamics of Fluids* (Wiley, New York, 1966), p. 135.
11. D. Mihalas and B. W. Mihalas, *Foundations of Radiation Hydrodynamics* (Oxford Univ. Press, London, 1984), p. 334.
12. E. E. Lewis and W. F. Miller, Jr., *Computational Methods of Neutron Transport* (Wiley-Interscience, New York, 1984), p. 34.
13. R. D. Richtmyer and K. W. Morton, *Difference Methods for Initial-Value Problems* (Interscience, New York, 1967).
14. P. J. Roache, *Computational Fluid Dynamics* (Hermosa, Albuquerque, NM, 1972), p. 237.
15. G. A. Sod, *J. Comput. Phys.* **27**, 1 (1978).
16. O. Yasar, Ph.D. thesis, University of Wisconsin-Madison, December 1989; UWFDM Report No. 823, Fusion Technology Institute Library, 1500 Johnson Drive, Madison, WI 53706.
17. K.-H. A. Winkler, M. L. Norman, and M. J. Newman, *Physica D* **12**, 408 (1984).
18. K.-H. A. Winkler, M. L. Norman, and D. Mihalas, "Implicit Adaptive-Grid Radiation Hydrodynamics," in *Computational Techniques—Multiple Time Scales*, edited by J. U. Brackbill and B. L. Cohen (Academic Press, New York, 1985).
19. Department of Energy, DOE/DP-0069, April 1989 (unpublished).
20. G. A. Moses *et al.*, University of Wisconsin Fusion Engineering Program Report UWFDM-800, May 1989 (unpublished).
21. J. J. Duderstadt and G. A. Moses, *Inertial Confinement Fusion* (Wiley, New York, 1982).
22. J. J. MacFarlane, *Comput. Phys. Commun.* **56**, 259 (1989).
23. J. J. MacFarlane, G. A. Moses, and R. R. Peterson, *Nucl. Fusion* **29**, 27 (1989).
24. R. R. Peterson and G. A. Moses, "Plasma Channels for the Propagation of Ion Beams in LIBRA," Proceedings of the Beams '88 Conference, July 1988, Karlsruhe, FRG.
25. O. Yasar and G. A. Moses, *Comput. Phys. Commun.* **69**, 439 (1992).
26. O. Yasar and G. A. Moses, *Nucl. Fusion* **31**, No. 2, 273 (1991).